J Therm Spray Tech (2021) 30:1810–1826
https://doi.org/10.1007/s11666-021-01252-5

PEER REVIEWED

# Residual Stress Analysis of Cold Spray Coatings Sprayed at Angles Using Through-thickness Neutron Diffraction Measurement

**Kelvin Loke[1,2,4] · Zhi-Qian Zhang[3] · Sridhar Narayanaswamy[3] · Pak Keng Koh[4] · Vladimir Luzin[5] · T. Gnaupel-Herold[6] · Andrew Siao Ming Ang[7]**

Submitted: 5 November 2020 / Accepted: 3 August 2021 / Published online: 26 August 2021


**Abstract** This work deals with the comparison of the morphology of aluminum 6061 splats cold sprayed at various angles between computational finite element modeling predictions and experimental observations. Computational modeling of single-splats sprayed at various angles predicted that the highest shear stresses would occur at impact angle of 60-65°, while the highest interfacial equivalent plastic strains would be observed at 50° and both would decrease as the spray angle increases. The amount of interfacial-bonded material was also observed to decrease as the spray angle increases. The computational model was correlated with experimental data from neutron diffraction and x-ray diffraction methods, and experimental tensile adhesive strength test results. From both neutron and x-ray diffraction through-coating measurements, it was also observed that the residual stress profile of the coatings would be increasingly more negative from the coating surface toward the substrate interface, before becoming less negative from that point on. The data also suggested that the coating residual stresses are largely biaxial although there were suggestions of anisotropy for coatings sprayed at oblique angles of 50° and 70°, which was also predicted by the simulation model.

**Keywords** additive manufacturing · cold spray · neutron diffraction · residual stress · thermal spray · x-ray diffraction · XRD

✉ Kelvin Loke
lokelvin84@gmail.com

✉ Zhi-Qian Zhang
zhangz@ihpc.a-star.edu.sg

✉ Andrew Siao Ming Ang
aang@swin.edu.au

1 ST Engineering Land Systems Ltd, Singapore, Singapore

2 School of Science and Technology, Singapore University of Social Sciences, Singapore, Singapore

3 Institute of High Performance Computing, A*STAR Research Entities, Singapore, Singapore

4 ECK Pte Ltd, Singapore, Singapore

5 Australian Nuclear Science and Technology Organisation, Lucas Heights, NSW, Australia

6 NIST Center for Neutron Research, Gaithersburg, MD, USA

7 Surface Engineering for Advanced Materials (SEAM), Swinburne University of Technology, Melbourne, VIC, Australia

## Introduction

Cold spray is a kinetic energy process that involves the use of high-velocity gasses, usually nitrogen, helium or compressed air, exiting from a "de Laval" nozzle with a converging-diverging internal geometry at velocities of more than Mach 1. Powder particles of sizes around 1-50 μm in diameter are then injected into this gas stream and are projected from the nozzle at particle velocities of more than 500 m/s onto the substrate surface (Ref 1). Previous works have shown that build-up is successful only if the powder particles attain a certain "critical velocity" (Ref 2). This critical velocity is dependent on equipment parameters such as gas pressure and gas temperature, as well as powder morphology and material properties. The cold spray build-up mechanism occurs only at velocities above this critical velocity (Ref 3). However, the mechanism of coating bonding is still not fully understood, and several researchers have suggested that a mixture of mechanisms were responsible for the bonding of coatings, mainly mechanical interlocking (Ref 4) and metallurgical bonding

due to adiabatic shear instability powder particle–substrate interface (Ref 5).

There have been many research papers published on the topic of potential cold spray applications, especially in the field of aerospace materials, remanufacturing additive manufacturing. Previous work was also done on the application of amorphous aluminum coatings deposited using cold spray (Ref 6) for the corrosion protection of aluminum structures, which are commonly found on aircrafts. Champagne et al. (Ref 7) described the use of cold spray to deposit various types of aluminum-based alloys on magnesium alloys as a promising, cost-effective and environmentally friendly technology to protect and repair magnesium aircraft components. Other works have been done to promote cold spray as a feasible additive manufacturing method (Ref 8, 9). Given that this is a line-of-sight process, it is important to explore effects of the torch spray angle relative to the built part.

Li (Ref 10), Gilmore (Ref 11) and Binder et al. (Ref 12) all reported that the deposition efficiency of cold spray can be correlated to the spray angle, and for the spraying of fine powders, the DE only varied by around 10% even at a spray angle of 45°. However, there are limited work done to establish the splat and coating formation during spraying at angles and the effects of spraying at angles, apart from deposition efficiency. This current work attempts to compare experimental observations using microstructure and tensile adhesive strength testing, with computational simulations of aluminum alloy deposits sprayed at different angles.

Previous works have been done to measure the eventual residual stresses within the cold sprayed build-up using neutron diffraction and XRD methods, with measured residual coating stresses to be equal to or lesser than -60MPa for aluminum and copper cold sprayed coatings (Ref 13, 14). A summary of research done with respect to residual stress measurement and analysis was compiled in Table 1. It was also to note that the cold sprayed samples in all those works were sprayed at 90° to the substrate surface, whereas there is little knowledge of the residual stress at different spray angles.

Thus, another aspect of this work is to explore the residual stress build-up using neutron diffraction and x-ray diffraction methods when the cold spray angle of deposition is varied. These computational models, physical experiments and diffraction measurements form a holistic approach to study the effect of spray angle for the cold spray deposition of aluminum alloys.

## Experimental

### Sample Preparation

The powder used for cold spraying is commercially available aluminum 6061 (Al6061) alloy from Valimet (USA), 325-mesh sieve grade, gas-atomised. All the Al6061 cold spray samples were made using the same batch of powder. Figure 1 is a representative SEM image of the morphology of the powder.

The cold spray equipment used in this work is the commercially available PCS-1000 high-pressure cold spray system from Plasma Giken (Japan). The system has a maximum spray temperature of 1000 °C and a maximum spray gas pressure of 5 MPa, with the capability to use either nitrogen or helium as the main process gas. The system currently is only fitted with one powder feeder unit. The cold spray gun was manipulated using a 6-axis industrial robot, and the general spray parameter is given in Table 2.

The Al6061 coatings were sprayed onto 6.5 mm thick substrates with dimensions 50 x 100 $mm^2$. While normally spraying is carried out in the direction perpendicular to the substrate surface, in the given study, samples were prepared using spraying under angles by tilting the substrate in a consistent manner (in the direction of the rolling direction of the substrate, RD, the 100 mm dimension) in respect to the spraying directions. In this way, a series of samples were sprayed at 50°, 70° and 90° angles, where 90° is the direction normal to the substrate surface. For these different spraying angles, the samples were sprayed until 0.3 mm thickness of coatings was achieved; the thickness which is close to the practical applications. In the case of the normal spraying (90°), an extra sample with 0.9 mm thickness was manufactured that allowed stress profiling through the coating thickness.

### Coating Characterization

Cross-sectioned samples for coating characterization were processed according to the ASTM E1920: Standard Guide for Metallographic Preparation of Thermal Sprayed Coatings (Ref 26); microscopy characterization was subsequently performed.

The adhesion or cohesion strength of the cold spray deposits was evaluated with accordance to the ASTM C633-01 test method (Ref 27). This test method can quantitatively determine the degree of bonding or adhesive strength of the coating deposit under a load normal to the substrate. The test starts with the cold spraying of one side of a 1-inch diameter stud made of Al6061 alloy, and then attaching this coated side to the face of another similar

**Table 1** Compilation of research done on residual stress measurements of cold spray coatings

| Refs. | Materials | Parameter varied | Trend observed | Measurement method | Stress state |
|---|---|---|---|---|---|
| (Ref 15) | Al-6082 | Number of spray passes, coating thickness, robot speed | Observations suggested that number of passes did not affect coating residual stress. However, the increase in the thickness of coating would result in a release of the residual stress near the interface | XRD | Compressive |
| (Ref 16) | Al, Cu, Ni, Zn, Ti, α-Fe, γ-Fe, Co | Particle impact velocity using different spray systems | Coating residual stresses were mainly determined from the peening during the splat impact onto the substrate surface and varied between materials due to different material yield stresses | Neutron diffraction | Compressive |
| (Ref 17) | Al | Powder and heat treatment annealing | Coating residual stress in Al is almost non-existent and was found to be possibly lower than the stresses induced by the splat peening onto the substrate surface during cold spraying. Annealing would almost completely decrease coating residual stress to zero | Neutron diffraction & XRD | Compressive |
| (Ref 18) | Al-6061 T6 | Substrate - Al & Mg | Coating residual stresses were found to be in slight compressive state and with similar stress profiles on both Al and Mg substrates. Through-thickness stress profiles and fit with the Tsui and Clyne empirical model would suggest a prevalence of kinetic over thermal effects of the cold spray process | Neutron diffraction | Compressive |
| (Ref 19) | Al-2024, Al-7075 | Main gas pressure, and temperature | Coating residual stress was observed to increase with gas pressure, and with decreasing temperature | XRD | Compressive |
| (Ref 13) | Cu, Al | Coating material and substrate material | Higher levels of plastic strain experienced by the coating material would result in higher levels of coating residual stress, due to the higher impact pressure from the denser materials. Residual stresses were demonstrated to accumulate from the results of kinetic effects rather than from thermal effects | Neutron diffraction | Compressive |

**Table 1** continued

| Refs. | Materials | Parameter varied | Trend observed | Measurement method | Stress state |
|---|---|---|---|---|---|
| (Ref 20) | Al-6061, Al-7075 | Particle impact velocity using different spray systems and different process gasses (Nitrogen & helium); different powder materials | Plastic properties of the coating material were found to be the most significant contributor to the compressive peening residual stress build-up within the coatings | Neutron diffraction | Compressive |
| (Ref 21) | Tantalum | Comparison between different residual stress measurement techniques | Residual stresses were found to be uniform throughout the thickness of the coating, and in both directions of the horizontal plane parallel to the substrate surface. In situ curvature measurement suggested that 85% of the residual stress built-up was from the kinetic effects of particle impact build-up on the substrate | Hole-drilling & Curvature method | Compressive |
| (Ref 22) | CP Al, Al-7075 | Comparison between experimental and modeling of residual stress | The FEM correlates well with experimental data to show that compressive residual stresses were induced by the peening effect during cold spray process. The study also finds that a longer coating duration and higher process temperature would play a significant role in relieving the residual stress | XRD | Compressive |
| (Ref 23) | Al | Comparison between different residual stress measurement techniques | The 3 methods used to measure residual stress showed a negative compressive stress in the coatings. The XRD and Almen gauge methods gave very similar results. The MLR method managed to show the presence of tensile stress peaks at interfaces between sequential passes within the coating through-thickness. This was attributed to stress formation between the added coating layer and the previous layer acting as a substrate | Almen gauge method, Modified Layer Removal Method, XRD | Compressive |

**Table 1** continued

| Refs. | Materials | Parameter varied | Trend observed | Measurement method | Stress state |
|---|---|---|---|---|---|
| (Ref 24) | Al, Cu, Ti | Comparison between different powder materials, substrate materials and pre-treatment | Residual stresses within the substrate imparted by pre-treatment such as grinding, and grit-blasting would be affected by the first layer of cold spray which could result in varying levels of annealing effect to impart some level of tensile stress relief. After that, the cold sprayed coating build-up could have a compressive or tensile residual stress, depending on the powder's material properties such as density and plastic deformation characteristics, and also the mismatch in coefficient of thermal expansion (CTE) between the powder and substrate. The difference in CTE between the 2 materials being proportional to the eventual thermal residual stress | Curvature method | Mainly compressive but tensile also observed |
| (Ref 25) | Ni-5%Al | Comparison between different thermal spray processes | Atmospheric plasma spray coatings were found to be tensile residual stress. Twin wire arc coatings were found to have nearly zero stress. High-velocity oxy-fuel coatings were found to have compressive residual stress. Cold spray coatings were also found to be compressive residual stress, although lower than HVOF | Neutron diffraction | Compressive |

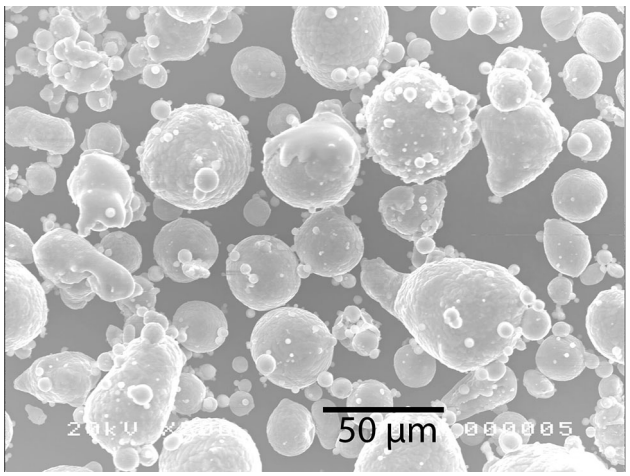


**Fig. 1** Valimet Al6061 alloy powder (Batch No. 07-8095S). Generally spherical morphology was observed

(uncoated) stud using epoxy glue (Masterbond EP15ND-2). Once the epoxy has cured (180 °C for 4 h), the bonded test studs were attached to jigs which were attached onto the tensile tester. The tensile tester used is the Universal Testing Machine (MTS SINTECH 65G), with all testing conducted at a crosshead speed of 1.0 mm per minute. The failure stress of the coating and the mechanism of coating failure are reported. For each deposition condition, 3 samples were measured, and the average bond strength is reported.

## Finite Element Simulation

To study the influence of impact angle on the development of residual stresses, simulations using finite element method (FEM) were carried out with Abaqus/Explicit based on the framework of Eulerian analysis (Ref 28-31). In the cold spray process, multiple layers are built up with impacting powder particles to form coatings. However, bonding in the cold spray process can be attributed to the initial interaction between the single particles impacting the substrate, and hence, the residual stresses at the particle–substrate interface are also significantly influenced by the single particle impact events. With this notion, this investigation was limited to the influence of the residual stresses induced by the single particle impact on the substrate, and the differences in residual stresses resulted from different impact angles. The influence of the impacts from the subsequent particles after the first initial layer is not studied in this work, but it is acknowledged to have cumulative influence on the residual stress distribution through the coating thickness build-up. This will be part of future work, which is currently in progress.

**Table 2** Cold Spray parameters used in this work

| Main gas type | Nitrogen |
|---|---|
| Main gas pressure | 4 MPa |
| Main gas temperature | 400 °C |
| Nozzle stand-off distance | 25 mm |
| Nozzle traverse speed | 100 mm/s |

The FEM model used in this work is shown in Fig. 2, with the refined regular mesh of mesh size $D/40$ ($D$ is the diameter of the particle) applied in the vicinity of the particle. The particle is assumed to be an ideal spherical shape with average diameter 40 µm, consistent with the average particle diameter used in the experimental work. The initial temperature of the powder particles and substrate is assumed to be room temperature, 300 K. To mimic the semi-infinite body of the substrate and eliminate the boundary effect in the simulations, the FEM model assumes the symmetric boundary conditions and isothermal condition are applied on the symmetric plane, and non-reflecting boundary condition and constant temperature condition of 300 K were imposed on other surface planes of the domain.

The constitutive material models for both powder particle and substrate employ the Johnson-Cook plasticity model, with the Mie–Grüneisen equation of state (Ref 3, 32, 33). The material properties used for the simulation model are shown in Table 3 (Ref 34). The simulations assume a thermal-mechanical coupling condition. Heat conduction is considered, and the temperature of the whole system is cooled down to 300 K.

The initial impact velocity magnitude of the powder particle is assumed to be 620 m/s, which is the critical velocity for bonding Al6061 particle to Al6061 substrate, and previously measure in physical experiments. The simulations apply different impact angles $\theta$ from 30° to 90°. In the simulation, the impact will start from time $t = 0$, and the simulation stops at $t = 800$ ns at which the kinetic energy is all dissipated and the system reaches the static status if the particle is deposited to the substrate. At the static status, the stress wave resulting from the impact will not affect the analysis of the simulation data.

## Residual Stress Measurement

### *Neutron Diffraction Method*

The neutron diffraction residual stress measurement of the cold sprayed Al6061 and the Al6061 substrate samples was carried out using the KOWARI strain scanner at the Australian Nuclear Science & Technology Organisation (ANSTO), OPAL research reactor facility. A neutron

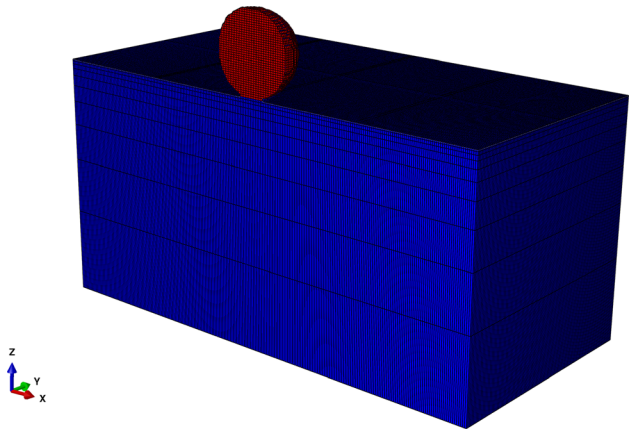

**Fig. 2** A 3D single-particle 1/2-symmetric model based on FEM in Eulerian framework using Abaqus. Blue color indicates the elements filled with substrate material, and red color indicates the powder material

**Table 3** Material Properties of Al6061 used in FEM modeling. (Unit SI: Kg m s K)

| | |
|---|---|
| Specific heat, J/K kg | 8.96E + 02 |
| Thermal conductivity, W/m K | 1.67E + 02 |
| Density, kg/m$^3$ | 2.70E + 03 |
| Shear modulus, Pa | 2.60E + 10 |
| $A$ | 3.24E + 08 |
| $B$ | 1.14E +08 |
| $N$ | 4.20E − 01 |
| $m$ | 1.34E +00 |
| $C$ | 2.00E − 03 |
| Reference strain rate | 1.00E + 00 |
| $C_0$ | 5.24E + 03 |
| $S$ | 1.40E + 00 |
| $\tau_0$ | 1.97E + 00 |
| Melting temperature, K | 8.80E + 02 |
| Transition temperature, K | 2.98E + 02 |

wavelength of $\lambda$ = 1.73 Å provided by the Si (400) monochromator at the take-off angle $2\theta_m$ of 79° was selected. It allowed to measure the strongest Al (311) reflection at the Bragg angle $2\theta$ of 90.4°. The high spatial resolution measurements with gauge volume of 0.3 x 0.3 x 20 mm$^3$ were done in three directions, the normal, transverse and rolling, to derive the residual stress of the cold sprayed coating Al6061 samples sprayed at 50°, 70° and 90° angles.

The measurement strategy was adapted for the different coating thicknesses as follows. For the thicker coating, a full stress profile was obtained through thickness of the cold sprayed coating (0.7 mm) and Al substrate (6.5 mm) in 0.3 mm steps. Obtaining stress profile not only in the coating but also in the substrate allowed indirect check of the stress in coating through the stress balance condition (the overall stress in the coating must be balanced by the overall stress in substrate). To isolate the residual stress associated with the cold spray process from pre-existing stresses in the substrate (e.g., from the rolling processes), similar stress measurements were done on an uncoated substrate, and this stress profile was subtracted from the stress profiles of the coated samples.

For the 0.3 mm thick coatings, the measurements in the substrate were less justifiable since higher accuracy of strain values would be required for the reconstruction of the stress in the coating indirectly. Therefore, only direct measurements in the 0.3 mm coatings were measured. Since coating thickness and gauge volume are both the same, 0.3 mm, only a measurement in a single point, which represents the average stress in coating, was made.

For each through-thickness depth, the two in-plane stress components, RD and TD, were calculated using the balanced biaxial plane stress state conditions and corresponding for Al (311) reflection diffraction elastic constants ($S_1 = -$ 5.16 TPa$^{-1}$, $\frac{1}{2}S_2$ = 19.57 TPa$^{-1}$). This method was confirmed in previous experiments on similar kinds of coatings (Ref 33).

### *X-ray Diffraction Method*

The residual stress profiling was also carried out by an alternative technique, the x-ray residual stress measurement method. Stress determination using this x-ray diffraction technique provides high spatial resolution measurements, and this method has been described previously (Ref 35). The measurements were conducted at the NIST Center for Neutron Research using an x-ray diffractometer equipped with a four-circle goniometer. The Cu-tube K-$\alpha$ radiation projected via a narrow vertical beam was employed to measure the Al (hkl 511/333) reflections. A combination of $\Omega$- and $\Psi$-angles as well as sample rotation is applied ( $\Psi$ tilts) in a way that ensures the x-ray beam projection remains parallel to the surface/interface. This allows the same through-thickness depth measurement and does not exceed the desired spatial resolution $\sim$ 0.1 mm.

The 'depth profile' was obtained by polishing and etching a small spot on the side surface (surface normal||TD); this ensures the removal of any mechanical damage. X-ray measurements used a 0.2 mm x 3 mm beam projected parallel to the edge of the sample, see Fig. 3. After a series of $\Psi$ tilts that sample was translated by 0.08 mm (0.12 mm for the sample with the largest thickness), with the beam spot now illuminating an area at a larger depth. The transition zone to the substrate and the substrate

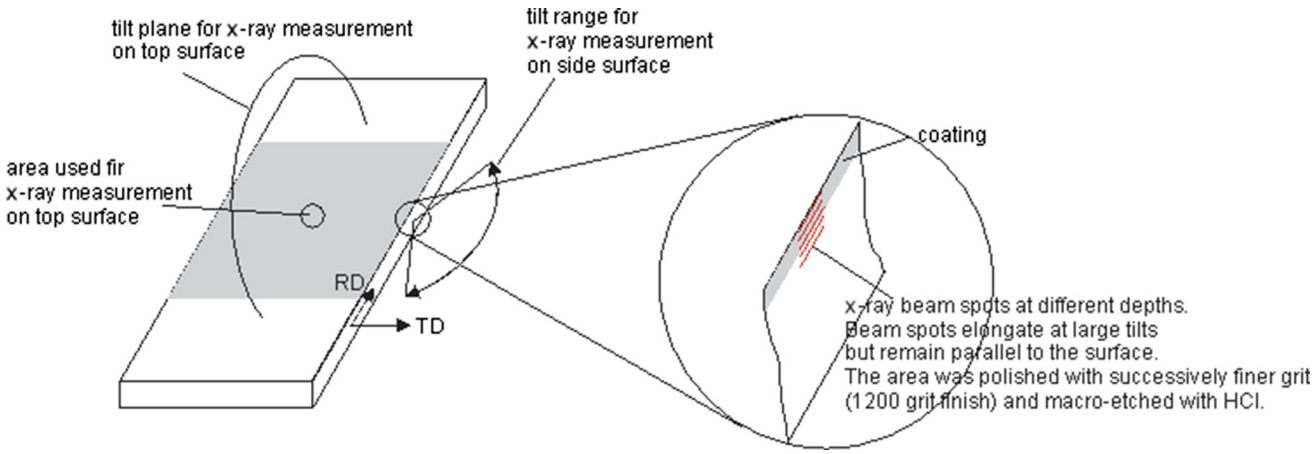


**Fig. 3** Directions and measurement locations used for the x-ray diffraction residual stress measurements. 'RD' refers to the Al 6061 substrate's rolling direction

itself was challenging to measure because of texture and grain size in the original Al6061 substrate. This 'depth profile' can be interpreted as such if the relief of the TD stress component on the side surface does not affect the stress parallel to RD. Note again that the side surface is normal to TD and that TD stress component here must be zero.

Finally, the stresses in all samples were measured on the surface in the center of the sprayed area using a classical $\Psi$ tilt scan mode with large beam. The x-ray residual stress measurements were made in the same samples studied previously using the neutron diffraction method, the 50°, 70° and 90° spray angles.

## Results and Discussion

### Finite Element Modeling of Splat Deformation at Different Spray Angles

*Influence on Residual Stress*

The FEM model described above was employed to study the material behavior between the powder particle and substrate. The simulations were carried out for cold spraying at $\theta = 30^\circ + n \times 5^\circ, n = 0\text{to}12$, respectively. The contour plots of equivalent plastic strain (PEEQ), temperature and von Mises stress under impact angles 40°, 50°, 70° and 90° are illustrated in Fig. 4, 5 and 6. The results are sampled at the time $t = 70\text{ns}$ after impact, at which the localized deformation, and the localized heating due to the extremely significant plastic deformation can be clearly observed.

The simulation results showed that if the impact angle is too small, the particle would have difficulty to be deposited onto the substrate, and the strain and stress fields will be minimal as seen for impact angles= 40° in Fig. 4(a), 5(a) and 6(a). This can also be explained by observing Fig. 4(b), 5(b) and 6(b) when the impact angle is increased to 50°, which clearly show the extremely large shear deformation appearing not only at the particle–substrate interface to form interfacial jetting, but also within the particle. This large plastic deformation generates the heat and elevated localized temperature within the particle material to more than 600 K; this is close to the melting temperature of the Al6061 material. During this impact event, the thermal softening effect of the Al6061 material is very significant; therefore, the material loses its strength in the shear band region and the particle consequently splits apart at small impact angle causing non-adhesion. Henceforth, only a small portion of the Al6061 particle can be deposited if the impact angle is smaller than 45°. If the impact angle is larger than 50°, the impacting Al6061 particle has more likelihood to bond successfully to its substrate. The deposited Al6061 particle mass portion is given in Fig. 7(a), which demonstrated that at small impact angles lower than 45°, the deposition is not efficient. In other words, economical cold spray deposition of Al6061 material occurs at spray angles larger than 50°.

Increasing the impact angle will reduce the shear deformation inside the particle, which can be explored by comparing the PEEQ contour plots in Fig. 4(b-f) and temperature contour plots in Fig. 5(b-f). This shear band gradually becomes inconsequential when the impact angle is larger than 65° and does not pose a detrimental effect to deposition efficiency.

The von Mises stress contour plots in Fig. 6 demonstrate that the stress field is inhomogeneous within the particle. It is noted that there are difficulties to compare the simulated residual stress solutions with the experimental residual

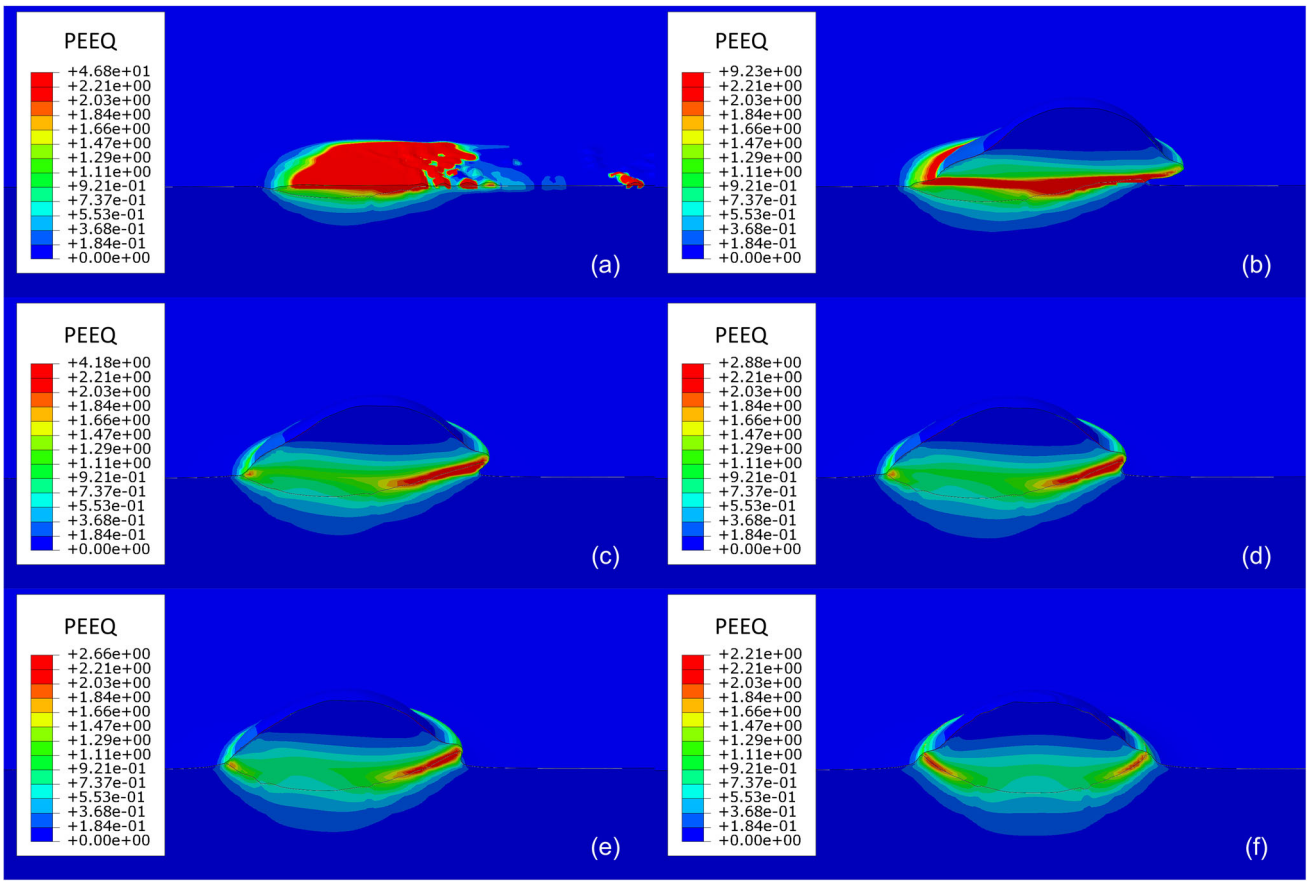


**Fig. 4** Contour plots of the simulation results of equivalent plastic strain (PEEQ) under impact angles (a) 40°, (b) 50°, (c) 60°, (d) 65°, (e) 70°, (f) 90°. Sampled at 70 ns after impact. Splats are traveling from the top downwards toward the bottom left corner for splats impacting at angles

stress measurement in the later part of this paper because the sampling location of the stress has a very significant influence on the stress magnitude. In this study, the volume averaging, which is often used in homogenization, was employed to post-process the data to generate the overall residual stress and strain of the particle after deposition, and to study the influence of the impact angle on the residual stress magnitude. The volume averaging of the stress component was calculated using the following equation:

$$\overline{\sigma}_{ij} = \int_{\Omega_p} \sigma_{ij} \mathrm{d}V \int_{\Omega_p} \mathrm{d}V \qquad \text{(Eq 1)}$$

where $\sigma_{ij}$ is the stress component, and $\Omega_p$ is the particle volume domain. Using the volume-averaged stress component $\overline{\sigma}_{ij}$, one can compute the volume-averaged von Mises stress $\overline{\sigma}_{vm}$ and shear stress $\overline{\sigma}_s$. The volume averaging of plastic strain $\epsilon_p$ and temperature $T$ can also be performed using the similar method. The shear stress was calculated using the following equation:

$$\overline{\sigma}_s = (\overline{\sigma}_1 - \overline{\sigma}_3)/2 \qquad \text{(Eq 2)}$$

where $\overline{\sigma}_1$ and $\overline{\sigma}_3$ are the volume-averaged maximum and minimum principal stress, respectively, which are calculated using the volume-averaged stress components.

The volume-averaged plastic strain is shown in Fig. 7(b), and the volume-averaged von Mises stress and shear stress are plotted in Fig. 7(c). Only the cases where the whole particle can be deposited were shown. It can be clearly seen that the volume-averaged plastic strain at smaller impact angles is larger, which is consistent to the PEEQ contour shown in Fig. 4. The plastic strain would decrease sharply from impact angles 50° to 70° and show moderate decrease from 70° to 90°. In the volume-averaged stress solution, the turning point is more obvious; from Fig. 7(c), the residual stress shows a significant change from the impact angles between 70° and 75°. The residual stress in the impact angle $> 70°$ is also seen to be much smaller than that in the impact angle $\leq 70°$. From the result in Fig. 7(c), one can also find that the residual von Mises stress is almost equal to the residual shear stress in

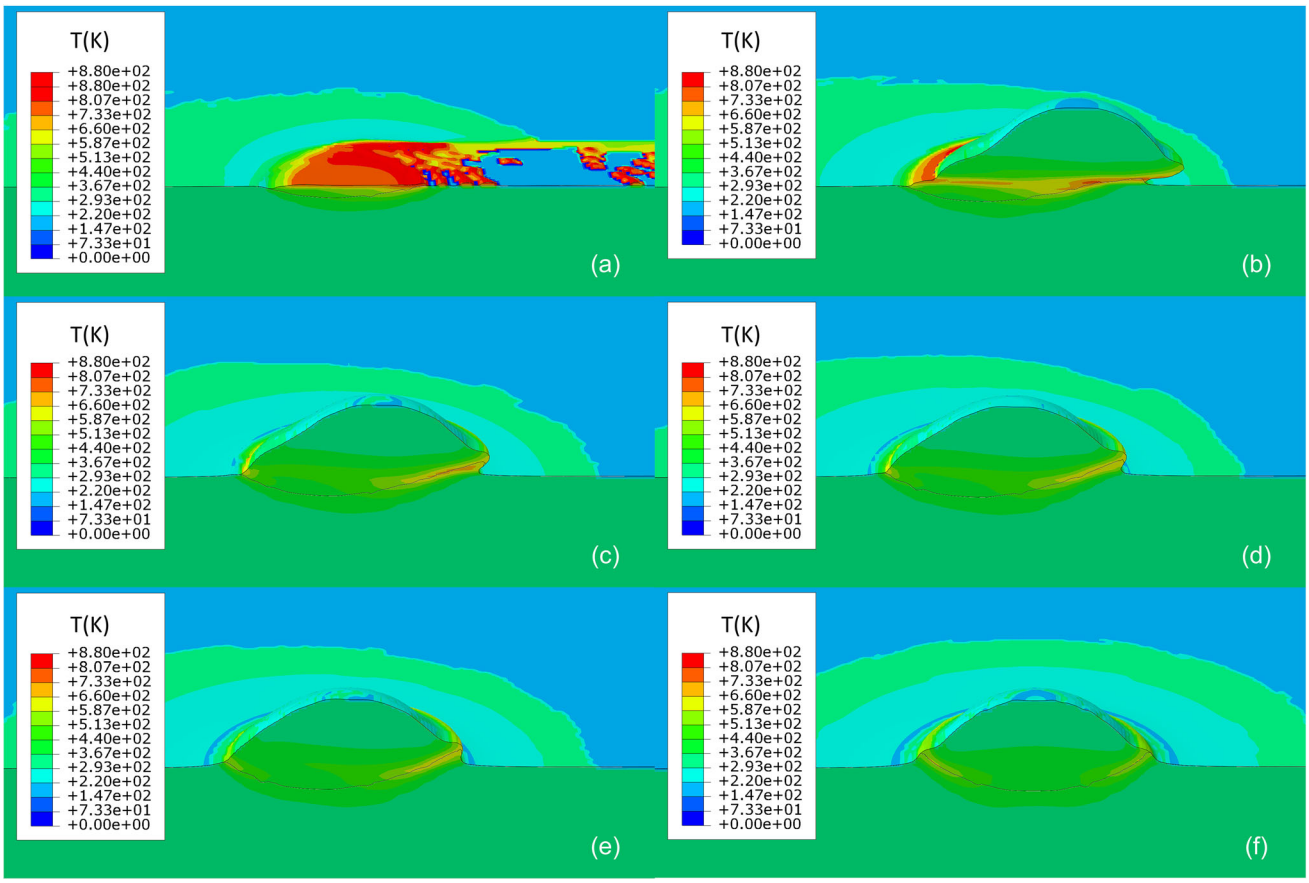


**Fig. 5** Contour plots of the simulation results of temperature (K) under impact angles (a) 40°, (b) 50°, (c) 60°, (d) 65°, (e) 70°, (f) 90°. Sampled at 70 ns after impact. Splats are traveling from the top downwards toward the bottom left corner for splats impacting at angles

the impact angle $\leq 70°$, indicating that in this case, the deformation of the particle is dominated by shear. In the case of impact angle $> 70°$, the shear deformation attenuates significantly, shown by the significant difference between the residual shear stress and von Mises stress in Fig. 7(c).

*Influence on Bonding Strength*

It is widely accepted that adiabatic shear instability is a major bonding mechanism in the cold spray process (Ref 3, 30, 32). In this study, it is proposed that the bonding strength can be correlated to the amount of interfacial-bonded material at the particle–substrate interface, which can be controlled by the spraying angle. This assumption is based on the findings that this bonded material occurred under adiabatic shear instability with significant localized plastic deformation and high localized temperature.

The volume fraction of the interfacial-welded material can be visually identified as the material colored in red on the temperature contour plots, indicating the material is near its melting point (See Fig. 5). A volume fraction of the interfacial-welded material in respect to the original particle volume is calculated and plotted in Fig. 7(d). This was calculated using the criterion that the amount of material at the splat-interface where the temperature is higher than 90% of the highest temperature generated at time $t = 70$ ns after impact. Most significantly, Fig. 7(d) showed that the interfacial-welded material amount decreased with increasing spray angle. This observation implies that the cold spray coating's bond strength is strongly correlated to its deposition spray angle. It is postulate that the increase in total volume of interfacial-bonded material will improve bond strength, though there will be a trade-off of reducing the deposition efficiency.

## Experimental Observations of Splats and Build-ups Sprayed at Angles

Microstructure analysis observed that voids were present, especially at the particle bases, with closure of the voids at the particle peripheries/interfacial jetting zones. This is in

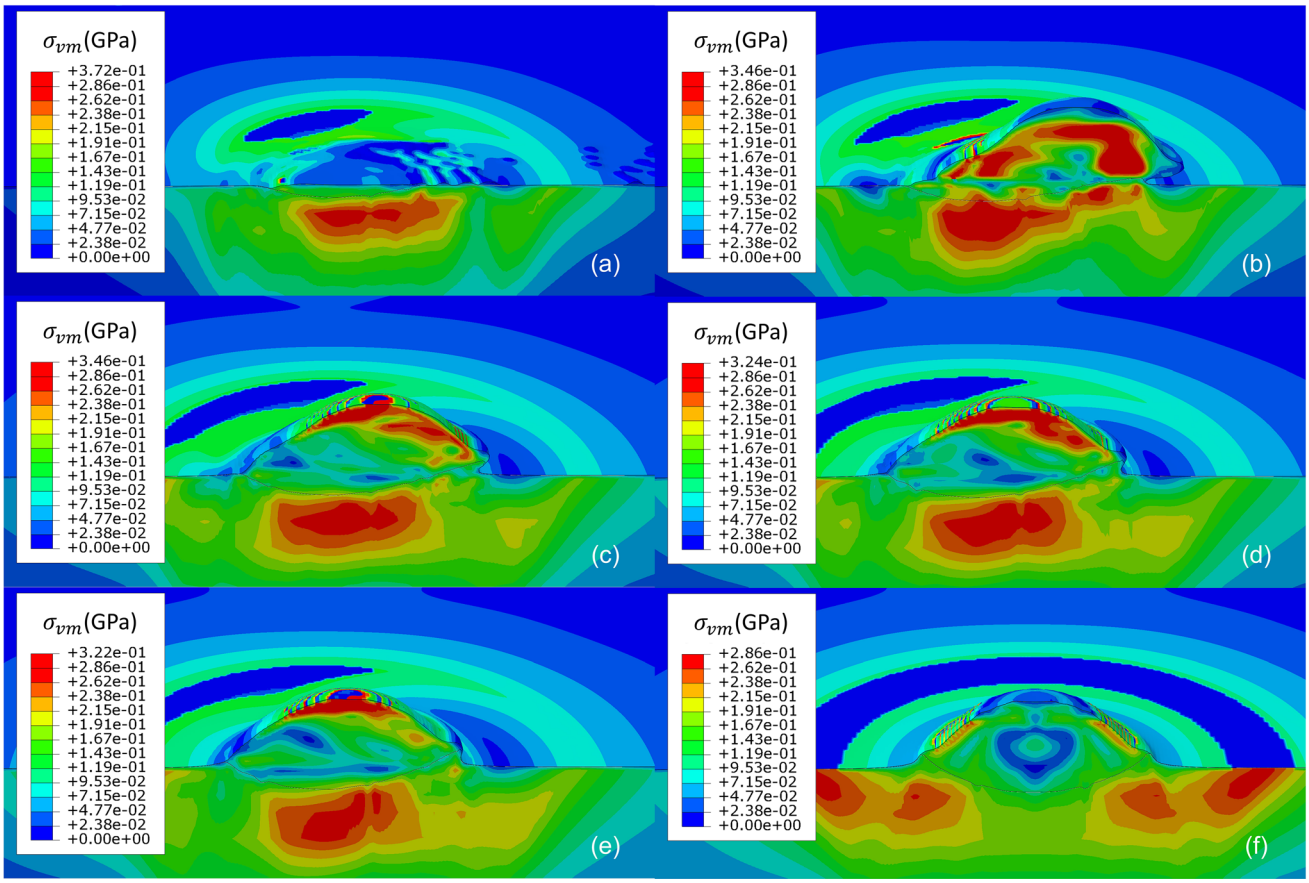


**Fig. 6** Contour plots of the simulation results of von Mises stress (GPa) under impact angles (a) 40°, (b) 50°, (c) 60°, (d) 65°, (e) 70°, (f) 90°. Sampled at 70 ns after impact. Splats are traveling from the top downwards toward the bottom left corner for splats impacting at angles

line with the modeling simulations shown earlier. Figure 8 shows the cross-sectional microstructures of built-up coatings sprayed at 40°, 60° and 90° spray angles. No visible melting of the substrates or at the inter-splat boundaries was observed in all 3 samples. The flattening ratio of the splats was observed to increase significantly as the impact angle changes from 90° to 40°, consistent with the single-splat simulations and how the single-splats were predicted to deform upon impact. Porosities were observed in all 3 spray angle samples. It was also observed that the build-up rate of the sample sprayed at 40° is extremely slow and decreasing from the 90° spray angle (Fig. 9), which is in line with results observed by Koh (Ref 36). From the microstructure, it also appears that the 40° sample has larger macro-porosities ($> 50$ μm), although all 3 samples were observed to contain porosities ($< 50$ μm).

## Tensile Adhesive Bond Strength Testing

Tensile adhesive bond strength testing was conducted for coating samples sprayed from 40° to 90° at 10° intervals. The average adhesion bond strength dependence on the spray angle is shown in Fig. 10. Although the strength values were determined with relatively large error bars, there is a trend in the dataset. Notably, the tensile adhesive strengths of the Al6061 cold sprayed coating sprayed at 60° angle reached the highest value of $\sim$ 60 MPa. This is at least 30% greater than the value for the coatings deposited at 90° spray angle. Thus, the overall results imply that despite the usual practice of maintaining 90° spray angle relative to the substrate, will not necessarily result in the best adhesive bond strength but instead yielded the lowest bond strength value of approximately 45 MPa. However, this possible increase in adhesion bond strength comes as a direct trade-off in terms of deposition efficiency and relative spray time to achieve the required thickness.

This effect appears to find explanation in our simulation results: with decreasing spray angles, the volume of 'effective' interfacial-bonded material increases and leads to improvements in the adhesion bond strength. The actual bonding strength of the macroscopically thick coating is ultimately influenced by many other factors, such as the

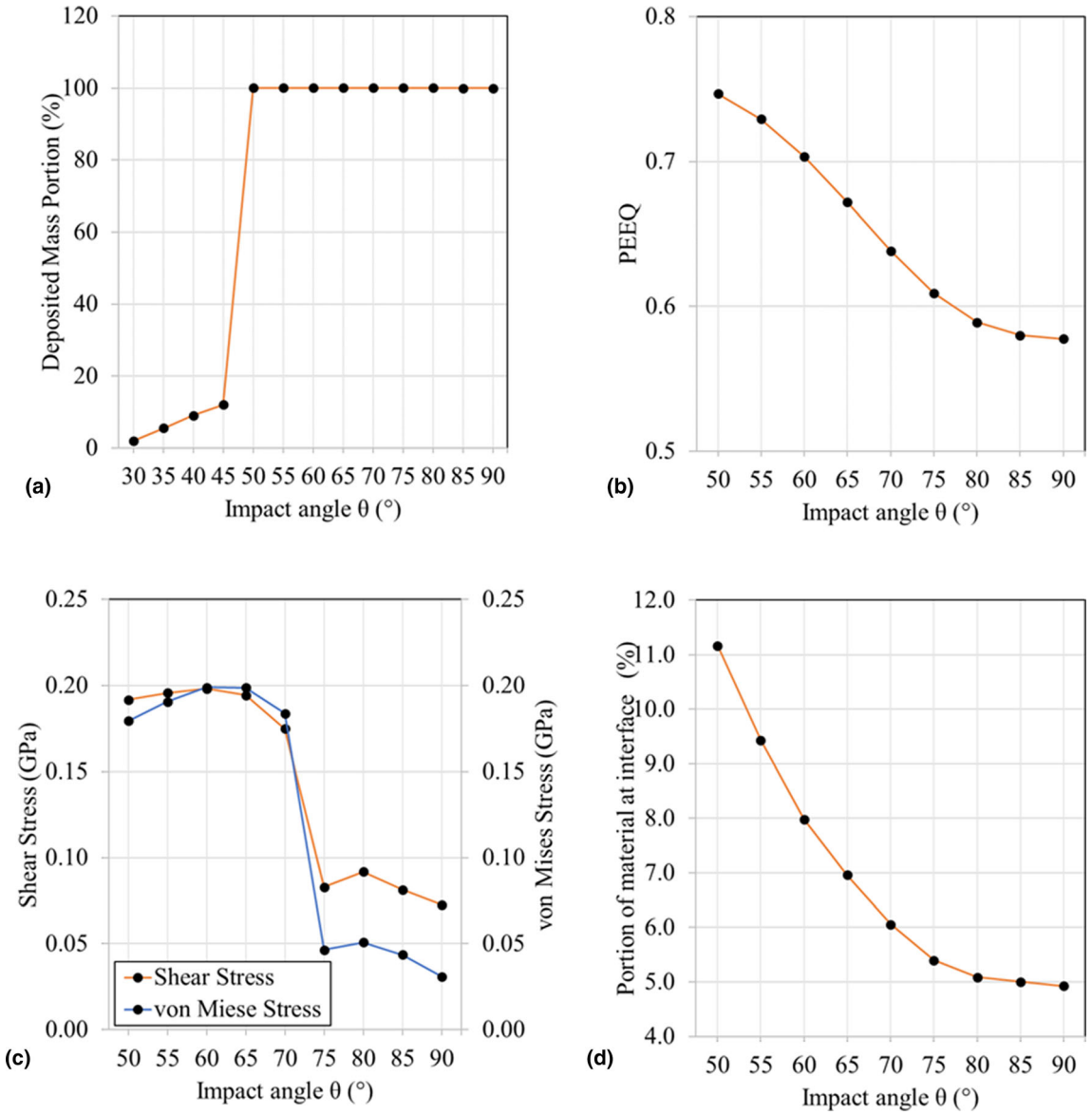


**Fig. 7** The simulation results versus impact angle. (a) Deposited mass portion of single powder particle upon impact, (b) volume-averaged equivalent plastic strain, (c) volume-averaged shear stress and von Mises stress versus impact angle and (d) portion of particle material at the particle–substrate interface. Solutions in (a) (b) and (c) are sampled after the whole system cools down to 298 K. Solutions in (d) are sampled t = 70 ns after impact

microstructures and defects, which were not considered in the current FEM model since this was a single particle simulation. However, the proposed micromechanical mechanism and the experimental data do provide a general explanation to the established relationship between the spray angle and coating bond adhesive strength. A multi-particle simulation, most likely, would be able to provide a qualitative prediction model of the bonding and trend under different cold spray process parameters and conditions.

## Residual Stress Analysis

To understand the macroscopic effect of spray angles on its influence on the development of Al6061 coating residual stress, two methods of through-thickness residual stress measurement were used. The two alternative techniques, the neutron and the x-ray diffraction method were applied with a possibility to countercheck the results.

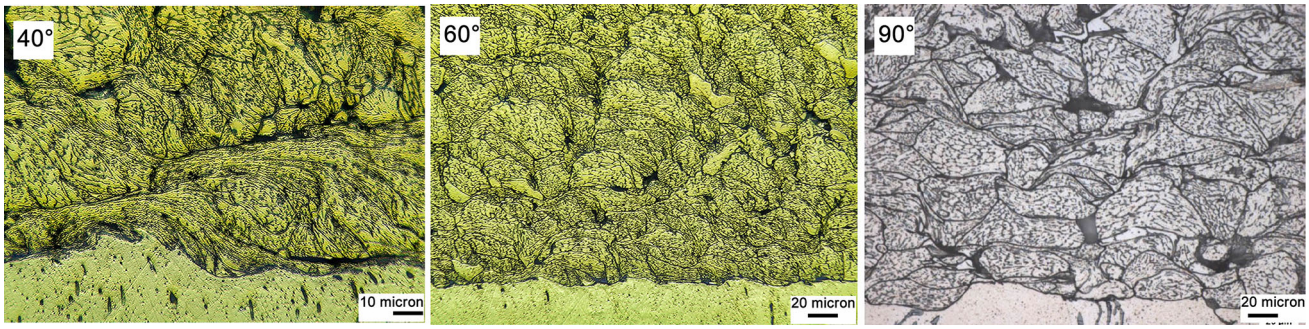


**Fig. 8** Cross-sectional microstructures of cold sprayed aluminum 6061 sprayed at spray angles of 40, 60 and 90° (non-grit-blasted). Etched with Keller's reagent

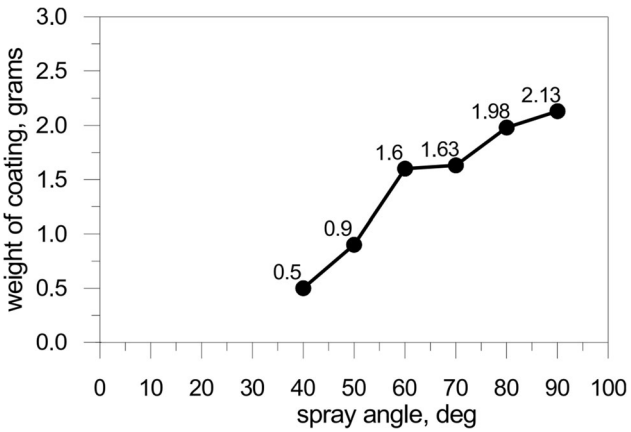


**Fig. 9** Weight of aluminum 6061 coating obtained at various spray angles per pass, while all other spraying conditions were identical (Ref 36)

### *The 700 μm Thick Coating*

The 700 μm thick coated sample provides a possibility to investigate the reliability of the experimental data since stress data are available both for the substrate and coating. The basis of the analysis is the Tsui and Clyne's analytical model that predicts the residual stresses in progressively deposited coatings (Ref 37). Through-thickness neutron stress measurements from substrate to coating and the model stress profile fitting the experimental data are shown in Fig. 11, while the same model data are matched against the x-ray stress measurement data (Fig. 11b). The model assumes stress generation through the deposition stress mechanism (Ref 37), while any thermally generated thermal mismatch stress is absent because there are no differences in the thermal expansion coefficient of the coating and substrate—they both are Al6061. In the case on neutron data, a stress balance was achieved within the entire coating-substrate system. The two stress measurement techniques and the model demonstrate general agreement for the stress in the 700 μm thick cold sprayed Al6061 coating: the residual stress mode is in compression with typical magnitude of − 40 MPa. Similar magnitudes of the compressive stresses were found previously in the Al6061 coatings produced by cold spray (Ref 20). Although only a single direction was measured by x-rays, RD, the neutron data for RD and TD undoubtedly confirm that the stress state is truly equi-biaxial, there is no anisotropy between RD and TD. This is expected due to the symmetry of particle deposition that arises from the 90° spray angle.

Under scrutinous examination, however, it could be also noticed that both neutron and x-ray measurement points close to the surface do not exactly follow the model line that predicts the tendency to be more negative at the surface. Contrary to model predictions, it appears that top the 200-300 μm layer has the opposite, positive, stress gradient. It can be explained by the different thermo-mechanical history of the top layer: it is much less peened as there are no subsequent incoming particles, and hence, this top layer did not experience the same steady-state regime during coating build-up. In many conventional XRD residual stress studies, this part of the deposit is often removed via grinding and polishing to create a flat profile required for measurement. Hence, this trend is not commonly reported within the literature.

### *The 300 μm Thick Coating*

Cold sprayed samples deposited to 300 μm thickness were made by 50°, 70° and 90° spray angles relative to the substrate surface and this allows the investigation into whether there is any directionality effect on the residual stress for the Al6061 coatings. As in the 700 μm thick coatings, the neutron data allow a separate analysis of both TD and RD stress components (although a single point was measured in the coating, representing the average stress in the coatings), while the x-ray data on the RD component

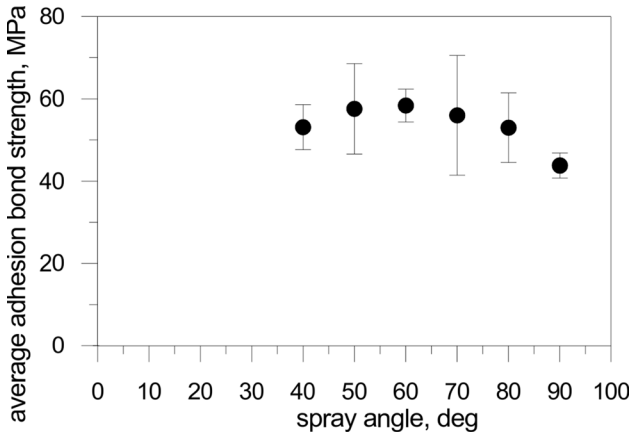


**Fig. 10** Comparison of average tensile adhesive strength values from Al 6061 coatings on Al 6061 substrates sprayed from 40° to 90° angles

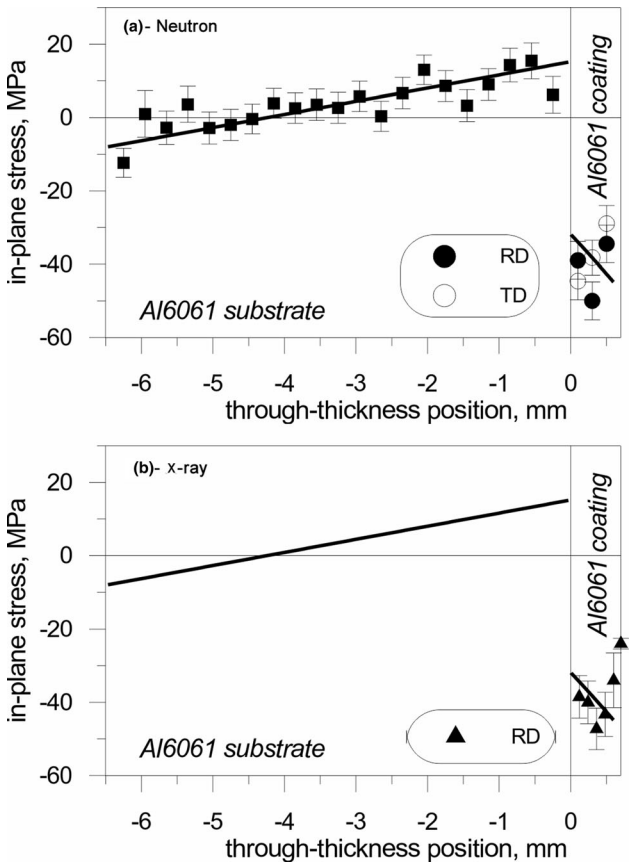


**Fig. 11** Residual stress profile through the 90° spray angle sample with coating thickness of 700 µm measured by (a) the neutron diffraction method and (b) the x-ray method

provide higher resolution stress profiling for the RD stress component. The x-ray measurements on the coating surface also allow analysis of RD and TD stress components

**Table 4** Residual stresses for the cold sprayed coating samples measured with neutron diffraction

| | Residual stress in RD, MPa | Residual stress in TD, MPa | Overall residual stress, MPa |
|---|---|---|---|
| Sample: 90° (700 µm thick), averaged over thickness | − 41 ± 3 | − 37 ± 3 | − 39 ± 2 |
| Sample: 90° (300 µm thick) | − 53 ± 4 | − 45 ± 5 | − 49 ± 3 |
| Sample: 70° (300 µm thick) | − 55 ± 5 | − 42 ± 5 | − 47 ± 4 |
| Sample: 50° (300 µm thick) | − 68 ± 5 | − 74 ± 5 | − 71 ± 4 |

independently and, therefore, to judge independently the bi-axiality of the residual stress state and, therefore, cross-check the neutron bi-axiality experiments.

The results of stress measurements in the 300 µm thick coatings are reported in Table 4 (for the average over thickness stress by neutrons, two directions), Table 5 (for the surface residual stress by x-rays, two directions) and Fig. 12 (the through-thickness stress resolved stress by x-rays, one direction, TD). The first fact to mention is that residual stress in all coatings is compressive, which is consistent with the results on the 700 µm thick coating and in accordance with expectations. Secondly, the results of both techniques show that the residual stress state in the two different principal directions, RD and TD, is not dissimilar considering finite statistical significance of the experimental data, although there are some slight differences for the non 90° spray angle samples. They are inconsistent in sign and of the same order of magnitude as the truly isotropic 90° spray angle samples. Also, though this experimental result seems counterintuitive and contradictive to the anisotropic splat deformation in an oblique fashion as shown by the simulation results and microstructure observations discussed earlier, it suggests that the final accumulated residual stress is mostly associated with the peening processes on the particle layers deeper than at the very top layer. In other words, although the very top deposited layer (i.e., $< 50$ µm) might have an anisotropic stress state, the deposition of the following layers will reset the stress state to isotropic since the coherent effect of peening on the underlying layers is apparently isotropic. However, this anisotropy cannot be detected even by the x-ray surface measurements because the very top layer is inevitably removed during surface preparation for the stress measurements. There is still a possibility that there might be some slight anisotropy, but the effect must be small, some 10 MPa, which is the accuracy of the current stress measurement capabilities,

**Table 5** Residual stress of the cold sprayed coatings measured by the x-ray diffraction measurement method on the top surface

| Surface Subs_RD\|phi=90 | Residual stress in RD, MPa | Residual stress in TD, MPa |
|---|---|---|
| Sample: 90° (700 μm thick) | − 24 ± 2 | − 30 ± 2 |
| Sample: 90° (300 μm thick) | − 38 ± 2 | − 37 ± 2 |
| Sample: 70° (300 μm thick) | − 16 ± 2 | − 27 ± 2 |
| Sample: 50° (300 μm thick) | − 50 ± 2 | − 60 ± 2 |

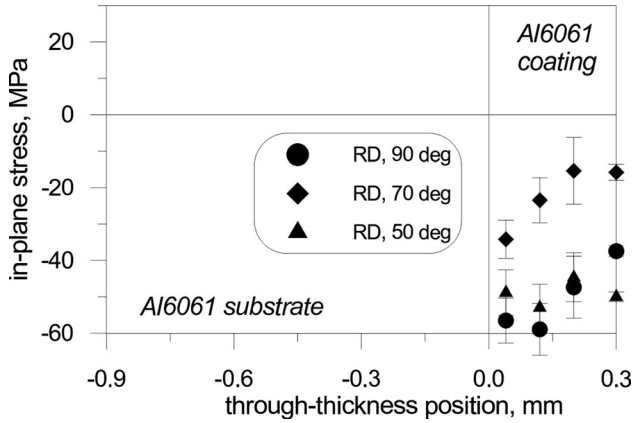


**Fig. 12** Residual stress profile measured in 300 μm thick coatings using x-ray diffraction

and this also requires higher positional accuracy measurements that are difficult to achieve. Thirdly, while the progressive layer deposition model predicts a negative gradient for the stress profile in coatings (as shown in Fig. 11), it appears that the stress profile in the top 300 μm follows the opposite trend with a positive gradient (Fig. 12). This is totally in agreement with the case of the 700 μm thick coating, where the topmost 300 μm layer exhibits a positive stress gradient, and though in this case, this effect is essentially valid for the whole thickness of the coating, while this effect can be addressed in the model by introducing a non-constant deposition stress parameter, due to the quantitatively small value of the stress gradient, some 3 MPa per 0.1 mm, the current analysis based on the overall (average) stress was chosen as the most reliable method for the comparative study of the effect of the spraying angle presented below.

*Effect of Spray Angle on the Stress State*

Although there is no experimental evidence of the stress state anisotropy (within our error bars), there is some experimental indication that the compressive stress magnitude does depend on the spray angle. For simplicity of assessment, the through-thickness x-ray data were averaged (see Table 6) to make them comparable with the neutron measurements and resultant data are plotted in Fig. 13. The measured coating residual stress has changed to − 70 MPa at the spray angle of 50°, as compared to the 70° and 90° samples with stress value approximately − 50 MPa. While our neutron measurement data tend to demonstrate this trend with both RD and TD components, the x-ray data points have somewhat of a lesser trend, also with some obvious bias in respect to the neutron data, specifically for the spray angle of 50° and 70°. This might be related to some inconsistencies of surface preparation: since surface polishing induces tensile stress in the near surface layer, this can potentially result in stress measurements biases and the stress values shift toward more tensile values if the affected layer is not fully removed by electropolishing. Thus, since the neutron diffraction technique is free of such effects, we consider our neutron data as a more reliable dataset for the purpose of comparing the average stress values. In summary, there is a dependence of compressive in-plane stress as well as the deposition stress seemingly observed with change of the spraying angle by means of the residual stress measurement using the neutron and x-ray diffraction methods.

This dependence follows a similar trend at the small angles as the coating tensile adhesive bond strength decreases at the low spray angle. Numerically, the effect is different though: while coating compressive residual stress magnitude increased by some 50% when the spray angle changes from 90° to 50°, the coating adhesive bond strength increases by some 30% over the same change of spray angle. From these collective residual stress measurements, one possible explanation for the higher coating adhesive bond strengths at lower spray angles could be due to higher compressive residual stress.

Overall, the simulation results and the experimental data by neutron diffraction and XRD demonstrate different aspects at different spatial scales of the stress accumulation during cold spray deposition if performed under tilting angle. In the scale of a splat, the simulation results show that at the smaller impact angles (40°-60°), the particle deformation is dominated by the extremely significant and localized shear deformation within the splat, which yields the remarkably higher residual stress eventually. The amount of localized shear deformation within the splat would decrease with increasing spray angles (70°-90°) along with the accumulated residual stress. In the macroscopic scale of the whole coating, as shown by the experimental data from neutron and x-ray diffraction residual

**Table 6** Summary of the measured average residual stress using two methods

| | Neutron diffraction Average residual stress, MPa | X-ray diffraction Average residual stress, MPa |
|---|---|---|
| Sample: 90°, 700μm thick | − 39 ± 2 | − 41 ± 3 |
| Sample: 90°, 300μm thick | − 49 ± 3 | − 55 ± 4 |
| Sample: 70°, 300μm thick | − 47 ± 4 | − 27 ± 4 |
| Sample: 50°, 300μm thick | − 71 ± 4 | − 49 ± 4 |

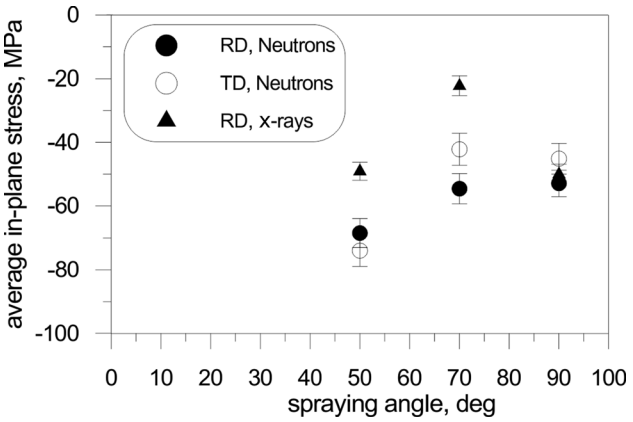


**Fig. 13** Measured residual stresses in Al6061 cold sprayed coating at different spray angles, in both traverse and longitudinal directions

stress measurements, all localized splat-scale stress fields are canceled to essentially an equi-biaxial stress state with only the in-plane stress component. The increase in the compressive residual stress from 70° to 50° observed experimentally corresponds to the similar jump in the shear stress and von Mises stress evident from the model data observed as the angle changes from 75° to higher values. More detailed measurements, e.g. in samples produced at 75°, 65°, 60°, 55°, can further corroborate this correlation. More experimental investigation is needed to understand details of the correlation between these observations and it is in progress.

## Conclusions

In this work, the effect of the spray angle was investigated for Al6061 alloy coating deposited on Al6061 substrate through experimental and modeling approaches. Simulation of a single-splat deposition event was carried out for a range of spray angles and predicted that the highest shear stresses would occur at impact angle of 60-65° while dropping sharply after 70°. Also, the highest interfacial PEEQ strains would be observed at 50° and decrease as spray angle increases. The simulations demonstrated that the interfacial-bonded material region decreasing with increasing spray angle. This was correlated with experimental data from tensile adhesion bond strength test, which showed that the highest bond strength occurred at 60° spray angle and the lowest at 90°. The higher tensile adhesion bond strengths observed for coatings at spray angles less than 90° could be associated with larger volume fraction of the high-temperature and high-plastic strain interfacial shear region (or interfacial-bonded material).

By using neutron diffraction and x-ray diffraction methods to measure the through-thickness residual stress on samples obtained by spraying under different angles, it allowed us to find that the cold sprayed coating's residual stresses are largely equal in TD and RD directions, thus, demonstration equi-biaxial stress state. There is a trend to have higher compressive residual stresses for the coating sample sprayed at 50°, while in the range of 70°-90°, the residual stresses remain constant. This correlates well with the FEM results that shows the shear stress increases sharply as spray angle decreased from 70° to lower values.

**Acknowledgment** The numerical simulation in this research is supported by the Agency for Science, Technology and Research (A*STAR) under the programme "Machining Learning Assisted Control of Metal Cold Spray and Shot Peening Processes (A1894a0032)". Dr Luzin and Dr Ang acknowledge the support by the Australian Research Council (ARC) under the Industrial Transformation Training Center project IC180100005 that is titled "Surface Engineering for Advanced Materials", SEAM. The neutron diffraction experimental work was supported through ANSTO user access program (proposal 7973).

## References

1. J.R. Davis, *Handbook of Thermal Spray Technology*, ASM International, Materials Park, 2004
2. A. Papyrin, V. Kosarev, S. Klinkov, A. Alkimov, and V. Fomin, Chapter 1—Discovery of the Cold Spray Phenomenon and Its Basic Features, *Cold Spray Technology*. A. Papyrin Ed., Elsevier, Oxford, 2007, p 1-32
3. H. Assadi, F. Gärtner, T. Stoltenhoff, and H. Kreye, Bonding Mechanism in Cold Gas Spraying, *Acta Mater.*, 2003, **51**(15), p 4379-4394
4. S. Kumar, G. Bae, and C. Lee, Deposition Characteristics of Copper Particles on Roughened Substrates Through Kinetic Spraying, *Appl. Surf. Sci.*, 2009, **255**(6), p 3472-3479
5. M. Grujicic, C.L. Zhao, W.S. DeRosset, and D. Helfritch, Adiabatic Shear Instability Based Mechanism for Particles/Substrate Bonding in the Cold-Gas Dynamic-spray Process, *Mater. Des.*, 2004, **25**(8), p 681-688
6. P.K. Koh, P. Cheang, K. Loke, S.C.M. Yu, and S.M. Ang, Deposition of Amorphous Aluminium Powder Using Cold Spray,

in *Proceedings of the International Thermal Spray Conference*, 2012, p 249-253
7. V.K. Champagne, The Repair of Magnesium Rotorcraft Components by Cold Spray, *J. Fail. Anal. Prev.*, 2008, **8**(2), p 164-175
8. G. Benenati and R. Lupoi, Development of a Deposition Strategy in Cold Spray for Additive Manufacturing to Minimize Residual Stresses, in Procedia CIRP, 2016, p 101-108
9. P. Dupuis, Y. Cormier, M. Fenech, and B. Jodoin, Heat Transfer and Flow Structure Characterization for Pin Fins Produced by Cold Spray Additive Manufacturing, *Int. J. Heat Mass Transf.*, 2016, **98**, p 650-661
10. C.J. Li, W.Y. Li, and H. Liao, Examination of the Critical Velocity for Deposition of Particles in Cold Spraying, *J. Therm. Spray Technol.*, 2006, **15**(2), p 212-222
11. D.L. Gilmore, R.C. Dykhuizen, R.A. Neiser, T.J. Roemer, and M.F. Smith, Particle Velocity and Deposition Efficiency in the Cold Spray Process, *J. Therm. Spray Technol.*, 1999, **8**(4), p 576-582
12. K. Binder, J. Gottschalk, M. Kollenda, F. Gärtner, and T. Klassen, Influence of Impact Angle and Gas Temperature on Mechanical Properties of Titanium Cold Spray Deposits, *J. Therm. Spray Technol.*, 2011, **20**(1-2), p 234-242
13. V. Luzin, K. Spencer, and M.X. Zhang, Residual Stress and Thermo-mechanical Properties of Cold Spray Metal Coatings, *Acta Mater.*, 2011, **59**(3), p 1259-1270
14. V. Luzin, K. Spencer, M.R. Hill, T. Wei, M. Law, and T. Gnaupel-Herold, Stress Profiling in Cold-Spray Coatings by Different Experimental Techniques: Neutron Diffraction, x-ray Diffraction and Slitting Method, in *International Conference on Mechanical Stress Evaluation by Neutron and Synchrotron Radiation, Materials Research Proceedings* 4, Kruger Natl Pk, South Africa, 2018, p 129-134
15. A. Moridi, S.M.H. Gangaraj, S. Vezzu, and M. Guagliano, Number of Passes and Thickness Effect on Mechanical Characteristics of Cold Spray Coating, *Proc. Eng.*, 2014, **74**, p 449-459
16. V. Luzin, K. Spencer, M. Zhang, and N. Matthews, Residual Stress in Coatings Produced by Cold Spray, *Mater. Sci. Forum*, 2014, **772**, p 155-159
17. W.B. Choi, L. Li, V. Luzin, R. Neiser, T. Gnaupel-Herold, H.J. Prask, S. Sampath, and A. Gouldstone, Integrated Characterization of Cold Sprayed Aluminum Coatings, *Acta Mater.*, 2007, **55**(3), p 857-866
18. M. Saleh, V. Luzin, and K. Spencer, Analysis of the Residual Stress and Bonding Mechanism in the Cold Spray Technique Using Experimental and Numerical Methods, *Surf. Coat. Technol.*, 2014, **252**, p 15-28
19. P. Cavaliere and A. Silvello, Processing Conditions Affecting Residual Stresses and Fatigue Properties of Cold Spray Deposits, *Int. J. Adv. Manuf. Technol.*, 2015, **81**(9-12), p 1857-1862
20. K. Spencer, V. Luzin, N. Matthews, and M.X. Zhang, Residual Stresses in Cold Spray Al Coatings: The Effect of Alloying and of Process Parameters, *Surf. Coat. Technol.*, 2012, **206**(19-20), p 4249-4255
21. O. Bailly, T. Laguionie, L. Bianchi, M. Vardelle, and A. Vardelle, Residual Stress Measurements in Cold Sprayed Tantalum Coatings, in *Proceedings of the International Thermal Spray Conference*, 2012, pp. 271-276
22. R. Ghelichi, S. Bagherifard, D. Macdonald, I. Fernandez-Pariente, B. Jodoin, and M. Guagliano, Experimental and Numerical Study of Residual Stress Evolution in Cold Spray Coating, *Appl. Surf. Sci.*, 2014, **288**, p 26-33
23. S. Rech, A. Trentin, S. Vezzù, J.-G. Legoux, E. Irissou, and M. Guagliano, Influence of Pre-Heated Al 6061 Substrate Temperature on the Residual Stresses of Multipass Al Coatings Deposited by Cold Spray, *J. Therm. Spray Technol.*, 2011, **20**(1-2), p 243-251
24. T. Suhonen, T. Varis, S. Dosta, M. Torrell, and J.M. Guilemany, Residual Stress Development in Cold Sprayed Al, Cu and Ti coatings, *Acta Mater.*, 2013, **61**(17), p 6329-6337
25. S. Sampath, X.Y. Jiang, J. Matejicek, L. Prchlik, A. Kulkarni, and A. Vaidya, Role of Thermal Spray Processing Method on the Microstructure, Residual Stress and Properties of Coatings: An Integrated Study of Ni-5 wt. % Al Bond Coats, *Mater. Sci. Eng. A*, 2004, **364**(1-2), p 216-231
26. ASTM E1920-03, *Standard Guide for Metallographic Preparation of Thermal Sprayed Coatings*, ASTM International, West Conshohocken, 2008
27. ASTM C633-01, *Standard Test Method for Adhesion or Cohesion Strength of Thermal Spray Coatings*, ASTM International, West Conshohocken, 2008
28. W.Y. Li, H. Liao, C.J. Li, G. Li, C. Coddet, and X. Wang, On high Velocity Impact of Micro-Sized Metallic Particles in Cold Spraying, *Appl. Surf. Sci.*, 2006, **253**(5), p 2852-2862
29. W. Li, Y. Min, W. Hui, and L. Hanlin, Effect of Mesh Resolution on the Particle Deformation during Cold Spraying by Eulerian Formulation, *Rare Metal Mater. Eng*, 2012, **41**, p 327-330
30. F.F. Wang, W.Y. Li, M. Yu, and H.L. Liao, Prediction of Critical Velocity During Cold Spraying Based on a Coupled Thermo-mechanical Eulerian Model, *J. Therm. Spray Technol.*, 2014, **23**(1-2), p 60-67
31. M. Yu, W.Y. Li, F.F. Wang, X.K. Suo, and H.L. Liao, Effect of Particle and Substrate Preheating on Particle Deformation Behavior in Cold Spraying, *Surf. Coat. Technol.*, 2013, **220**, p 174-178
32. G. Bae, Y. Xiong, S. Kumar, K. Kang, and C. Lee, General Aspects of Interface Bonding in Kinetic Sprayed Coatings, *Acta Mater.*, 2008, **56**(17), p 4858-4868
33. M. Saleh, V. Luzin, and K. Spencer, Evaluation of the Residual Stress in the Cold Spray Technique Using Smooth Particle Hyrodynamics Modelling and Neutron Diffraction, *Mater. Sci. Forum*, 2014, **777**, p 205-212
34. K. Saptaji and S. Subbiah, Finite Element Study of the Effect of Substrate Properties in Micro-cutting Thin Workpiece Materials, in *IOP Conference Series: Materials Science and Engineering*, 2016
35. T. Gnäupel-Herold, Formalism for the Determination of Intermediate Stress Gradients Using X-ray Diffraction, *J. Appl. Crystallogr.*, 2009, **42**(2), p 192-197
36. P.K. Koh, *Coating Deposition in Cold Spray Process, Engineering Doctoral Thesis*, Nanyang Technological University, Singapore, 2016. https://doi.org/10.32657/10356/66531
37. Y.C. Tsui and T.W. Clyne, An Analytical Model for Predicting Residual Stresses in Progressively Deposited Coatings Part 1: Planar Geometry, *Thin Solid Films*, 1997, **306**(1), p 23-33